

Microwave spectroscopic observation of distinct electron solid phases in wide quantum wells

March 15, 2022

A. T. Hatke, Yang Liu, B. A. Magill, B. H. Moon, L. W. Engel, M. Shayegan,
L. N. Pfeiffer, K. W. West, K. W. Baldwin

National High Magnetic Field Laboratory, Tallahassee, Florida 32310, USA

Department of Electrical Engineering, Princeton University, Princeton, New
Jersey 08544, USA

In high magnetic fields (B), two dimensional electron systems (2DESs) can form a number of phases in which interelectron repulsion plays the central role, since the kinetic energy is frozen out by Landau quantization. These phases include the well-known liquids of the fractional quantum Hall effect (FQHE), as well as solid phases with broken spatial symmetry and crystalline order. Solids can occur¹⁻⁸ at the low Landau filling (ν) termination of the FQHE series, but also within integer quantum Hall effects (IQHEs)⁹. Here, we present microwave spectroscopy studies of wide quantum wells (WQWs)¹⁰⁻¹⁴. The spectra clearly reveal two distinct solid phases, hidden within what in dc transport would be the zero diagonal conductivity of an integer quantum Hall effect state. Explanation of these solids is not possible with the simple picture of a Wigner solid (WS) of ordinary (quasi) electrons or holes.

Solid phases of carriers are insulators, owing to pinning by disorder, and are not easily distinguishable from other types of insulators by standard dc transport measurements, but rather by a characteristic resonance, at frequency f_{pk} in their microwave conductivity spectra^{5,9,15,16}. These resonances are understood as pinning modes^{5,16} in which pieces of the solid oscillate within the disorder potential, as diagrammed in Fig. 1(a). Pinning modes have been found both near the low ν termination of the FQHE series^{5,15} and within the ν -ranges of IQHE plateaus⁹. In the weak pinning picture¹⁷⁻¹⁹ f_{pk} increases when the shear modulus, C_t , decreases, for example by decreasing the density, n ²⁰. The inverse relation of f_{pk} and C_t is

because carriers associate more closely with minima in the disorder potential^{17–19}. Consistent with this picture, in wells narrower than those studied here⁹, a solid within the IQHE range shows a monotonic decrease of f_{pk} as ν moves away from the quantizing filling, which increases the charge density of the solid.

Here we report pinning modes whose f_{pk} exhibits an *upward step* as ν is decreased from 1, in contrast to the monotonic decrease of f_{pk} that was seen in narrower wells. The phenomenon is seen in WQWs, in which the effective electron-electron interaction is softened at short range due to the large growth-direction extent of the wave function. A wider well, or a larger n , cause the step to move closer to $\nu = 1$. We provide a natural interpretation, based on the sensitivity of f_{pk} to the properties of the solid, that the step signals a transition between different solids.

Our samples came from two WQW wafers with different width, w . Henceforth in this paper all n will be in units of 10^{11} cm^{-2} for brevity. One WQW has $w = 54 \text{ nm}$, depth of the 2DES from the top $d = 430 \text{ nm}$, and as-cooled $n = 2.42$. The other has $w = 65 \text{ nm}$, $d = 510 \text{ nm}$, and as-cooled $n = 1.52$. The data were taken with a charge distribution that is approximately symmetric about the well center (see Methods). Microwave data were taken using the set-up in Figs. 1(b) and (c) .

The spectra in Figs. 1(d)-(g) give an overview of the evolution of the resonance with Landau filling at different n for the two WQWs. We present results in terms of $\nu^* = \nu - 1$, where $|\nu^*|$ is nearly proportional to the quasi-particle or hole density. In the smaller- n states in Figs. 1(d) and (f), and also for the larger- n states in Figs. 1(e) and (g) with $\nu^* > 0$, resonances

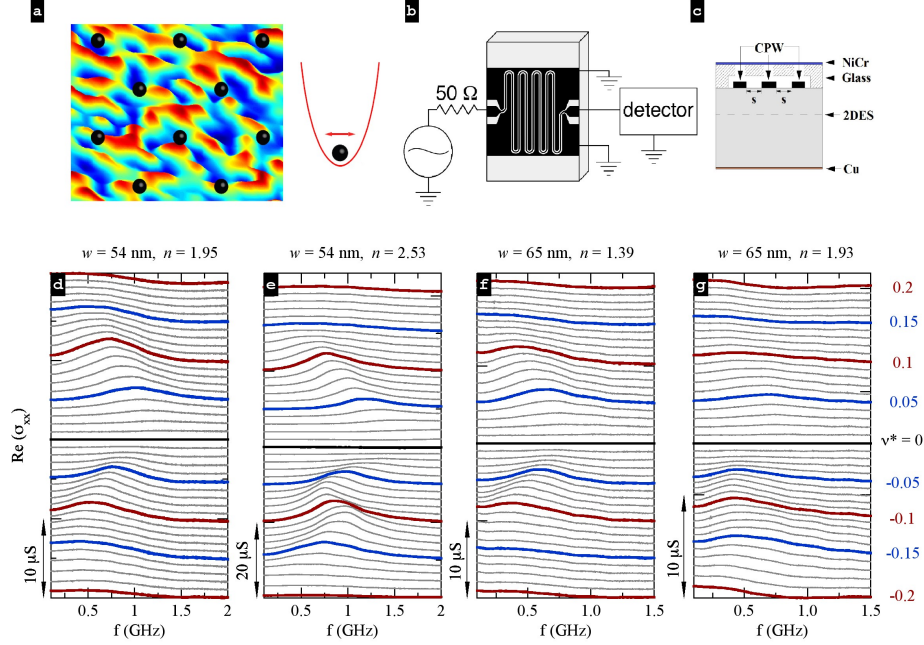


Figure 1: (a) Left: sketch of carriers (black) of an electron solid within the residual disorder potential which is shown by color (not to scale). Right: A piece (domain) of solid moves within a potential due to the disorder averaged over the domain, giving rise to the pinning mode studied here. (b) Schematic of the microwave setup. The source and detector are at room temperature. A coplanar waveguide (CPW) transmission line is patterned onto the top surface of the sample, with metal film of the CPW shown in black. (c) Side view of the sample (not to scale) shows the placement of the front and back gates and the metal film of the CPW. Slots of width s separate the center conductor and ground planes of the CPW. (d) and (e) Spectra (diagonal conductivity, $\text{Re}(\sigma_{xx})$, vs frequency, f) obtained from the 54 nm well with $n = 1.95$ and 2.53 , at several $\nu^* = \nu - 1$, marked on the right axis of (g). Successive spectra are offset upward by $1\mu\text{S}$ in (d) and $2\mu\text{S}$ in (e). (f) and (g) Spectra for the 65 nm well at $n = 1.39$ and 1.93 offset consecutively by $1\mu\text{S}$.

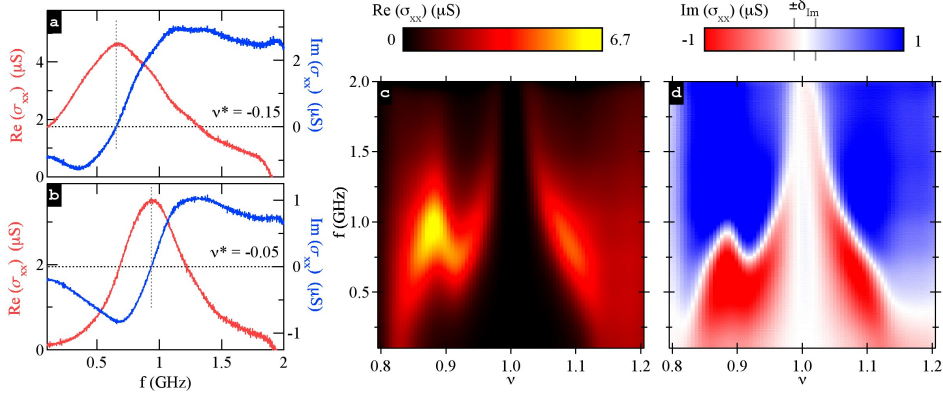


Figure 2: (a) and (b) Real (left axis), and imaginary (right axis), parts of conductivity σ_{xx} vs f at two fixed ν^* as marked, obtained from the 54 nm well at $n = 2.53$. Dotted vertical lines mark the zero crossing of $\text{Im}(\sigma_{xx})$ vs f , from which f_{pk} is determined. The error in $\text{Im}(\sigma_{xx})$, $\pm\delta_{\text{Im}} = \pm 0.08 \mu\text{S}$, includes random noise and slower variation in $\text{Im}(\sigma_{xx})$ vs f due to residual reflections near the sample mount. (c) and (d) Color images in the (f, ν) -plane for $\text{Re}(\sigma_{xx})$ and $\text{Im}(\sigma_{xx})$, respectively. The color scale in (d) is set such that the center of the white band is 0, and its extent in $\text{Im}(\sigma_{xx})$ is $\pm\delta_{\text{Im}}$. Thus the white band in the image traces out f_{pk} vs ν and its height is $\pm\delta(f_{\text{pk}})$.

develop as in Ref. 9: as $|\nu^*|$ increases the resonance forms, develops maximal absorption around $|\nu^*| = 0.08$ to 0.10 , and then fades away, all as f_{pk} *monotonically* decreases with $|\nu^*|$. The resonance development is different for the larger- n states with $\nu^* < 0$. In Figs. 1(e) and (g) f_{pk} decreases with decreasing ν^* but near $\nu^* \sim -0.08$ begins to *increase*. Further decrease of ν^* results in an increase of f_{pk} until $\nu^* \sim -0.12$, below which f_{pk} again decreases.

f_{pk} is extracted from the zero crossing of the imaginary conductivity, $\text{Im}(\sigma_{xx})$, vs f , as explained in Fig. 2. Figure 3 shows plots of f_{pk} vs ν^* at several n for the two WQWs. For the lowest- n traces, f_{pk} vs $|\nu^*|$ monoton-

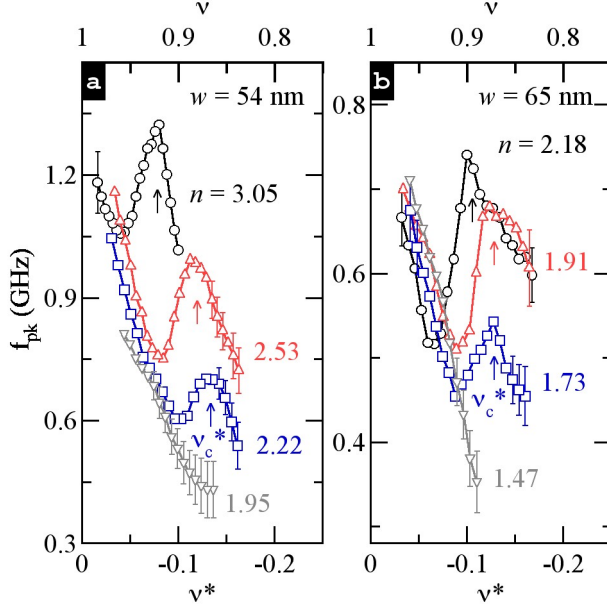


Figure 3: f_{pk} vs partial Landau level filling ν^* for the 54 nm (a) and 65 nm (b) wells at various carrier densities (n) as marked. Arrows mark ν_c^* , the ν^* of the local maxima in f_{pk} . Data points without an attached error bar have estimated error in f_{pk} that is smaller than $\pm 5\%$.

ically decreases, but for larger n a local minimum and maximum develop. The minimum and maximum move closer to $\nu^* = 0$ as n increases and are exhibited at lower n for the 65 nm sample.

We interpret the results in terms of a transition between two distinct solids. At the lowest n for both samples f_{pk} monotonically decreases with $|\nu^*|$. At larger n , the f_{pk} vs ν^* curves can be divided into two regions. In the smaller $|\nu^*|$ regions (closer to $\nu = 1$) f_{pk} vs ν^* tends toward the lowest- n curve, while in the larger $|\nu^*|$ regions, to the right of the local maximum in Fig. 3, f_{pk} vs ν^* is enhanced relative to the lowest- n curve. We take the enhanced f_{pk} as a characteristic of a solid which we call S2. It is distinct from S1, which is the only solid seen in the lowest n states of the samples,

and which in the larger n states is closer to $\nu^* = 0$. With increasing n the transition from S2 to S1 moves closer to $\nu^* = 0$, and the transition appears at lower n in the larger w sample. Screening of disorder by larger $|\nu^*|$, rather than a transition between solids, would produce a reduced f_{pk} for larger $|\nu^*|$, in contrast to the observed enhanced f_{pk} . Though we focus on the resonance for $\nu^* < 0$, we have, at some of the largest n , been able to see the step to enhanced f_{pk} as $|\nu^*|$ increases for $\nu^* > 0$ also. The transition thus appears to occur on both sides of $\nu = 1$, therefore S2 is favored by larger n , w and $|\nu^*|$.

We also perform dc transport measurements on the same wafers, and find that the solid-solid transition picture can underlie features found earlier¹¹ in dc transport. WQWs were recently found¹¹ to exhibit ν ranges that are not contiguous with the IQHE minimum centered at $\nu = 1$, but still have Hall resistance quantized at h/e^2 and vanishing dc longitudinal resistance (R_{xx}). These regions are called reentrant integer quantum Hall effects (RIQHEs)²³ and are due to insulating phases of the partially filled Landau level. At sufficiently high n , the RIQHEs appear near $\nu = 4/5$ ¹¹. The RIQHE range extends toward $\nu = 1$ as n is increased by gating, and eventually merges with the main IQHE plateau. The RIQHE was ascribed¹¹ to a WS, which can be favored²¹ over FQHE liquids in WQWs, owing to the softening of the effective electron-electron interaction at short range. The RIQHE sets in for $w/l_B \gtrsim 4$, where $l_B = (\hbar/eB)^{1/2}$ is the magnetic length.

Figures 4 (a) and (b) show plots of R_{xx} vs ν^* for the 54 and 65 nm wells at several n . Just closer to $\nu^* = 0$ than the minimum due to the RIQHE, the R_{xx} traces have peaks, both in Ref. 11 and in Figs. 4 (a) and (b), which

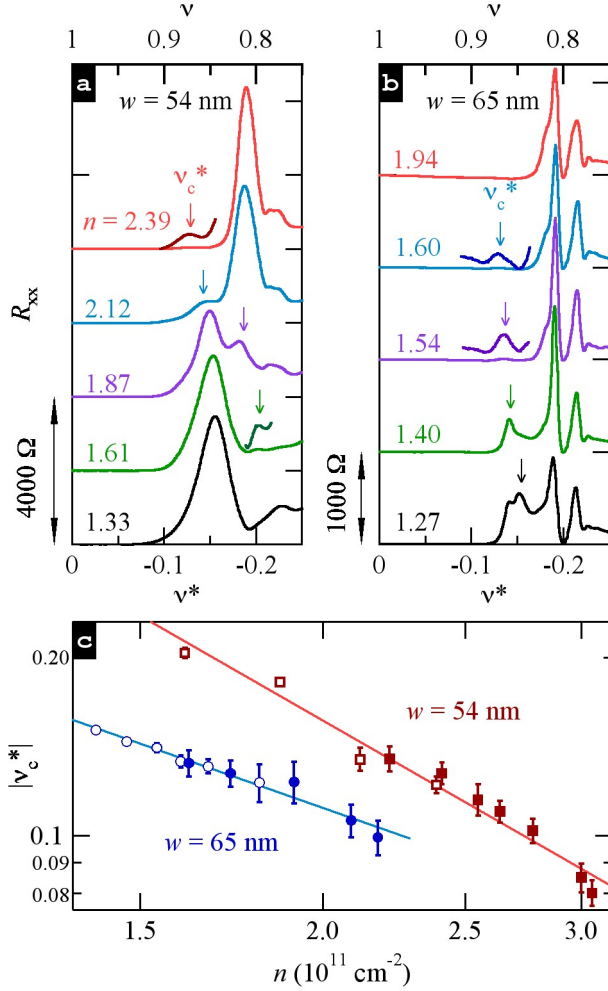


Figure 4: (a) and (b): Longitudinal resistance versus ν^* measured for the 54 nm (a) and the 65 nm (b) wells at different n as marked, vertically offset for clarity. Arrows mark ν_c^* , the critical partial filling factor. Where R_{xx} is small, the trace in the region of ν_c^* are duplicated and magnified 10 times for clarity. (c) $|\nu_c^*|$ vs n on a log-log scale deduced from dc transport measurements (open symbols) and microwave spectra (solid symbols) for the 54 nm (squares) and 65 nm (circles) wells. Power law fits of the form $\nu_c^* \propto n^{-\alpha}$ are also shown on the plot, where $\alpha = 1.35 \pm 0.1$ and 0.87 ± 0.07 for the 54 and 65 nm wells, respectively.

are denoted with arrows. With increasing n the ν^* of the peak increases as the RIQHE minimum deepens. At the highest n the peak vanishes as the RIQHE minimum merges with the main IQHE minimum. This peak in R_{xx} could be produced by domain-wall conduction at a phase transition^{11,22}.

To directly compare microwave and dc measurements we define the critical filling ν_c^* as that of the local maximum in the f_{pk} vs ν^* measurements and that of the n -dependent peak in R_{xx} vs ν^* , marked by arrows in Figs. 3 and 4. This results in continuous plots of ν_c^* vs n , as shown in Fig. 4(c), so that S2 can be identified with the dc RIQHE. The ν^* -ranges of ν_c^* vs n obtained from microwave and dc overlap at intermediate n and are remarkably consistent over the entire n range. Resonances for S2 set in at larger n than required to see the dc transport RIQHE, and can be seen at smaller $|\nu^*|$. When the RIQHE merges with the IQHE the R_{xx} peak at ν_c^* is no longer visible, even when the transition is clearly visible in f_{pk} . Pinning modes are not visible in the RIQHE ranges at larger $|\nu^*|$, possibly because uncondensed carriers are present which dampen the resonance.

Reference 15 reported evolution of the pinning mode with ν below the termination of the FQHE series, in quantum wells with $w = 50$ and 65 nm, but with much lower n ($\simeq 1$ and 0.5 respectively) than those studied here. For $0.12 < \nu < 0.18$, the spectra appeared irregular with multiple peaks, though well-defined peaks appeared above and below that range. In Ref. 15 that ν range was the same in each sample, and for $\nu \gtrsim 0.18$, the resonance was wave vector (q) dependent. The q dependence was found by comparing transmission lines of different slot width, s , $q \sim \pi/s$ (see Methods). Checking for q dependence in the present 54 nm WQW sample using $s = 80$ μm

we found none, with excellent agreement between the $s = 80 \mu\text{m}$ f_{pk} vs ν^* and the $s = 30 \mu\text{m}$ data shown in Fig. 3(a).

Theories^{7,24–26} have considered crystals of composite fermions (CFs). CFs are categorized by the number, $2p$, of vortices bound to a carrier. Theory predicts a series of distinct CF WS ($^{2p}\text{CFWS}$) phases with $2p$ increasing as ν decreases^{7,24}. The transition from $2p = 2$ to 4 occurs as ν goes from $1/5$ to $1/6$. Though 4C_t is predicted to soften near the transition, well within the $^4\text{CFWS}$ it is calculated to be a factor of ~ 2 larger than 2C_t , and would result in a lower f_{pk} in the $^4\text{CFWS}$. Identifying S2 as a $^2\text{CFWS}$ and S1 as a $^4\text{CFWS}$ would be consistent with the shear moduli predicted by Ref. 7. However, Ref. 7 predicts little sensitivity of the phase diagram to w , but we do observe dependence of ν_c^* on w and n .

Are there other possible interpretations for the two solids? A two-component bilayer WS can exist under certain conditions in a WQW^{12,13}, particularly if the subband gap, Δ , is small enough relative to the Coulomb energy, E_c . Such a two-component WS could have increased disorder and f_{pk} due to charge being pushed closer to the interfaces¹⁷, and would be favored by larger $|\nu^*|$, giving smaller carrier spacing, and by larger w . For the 54 nm well with typical $\nu_c = -0.1$, $n = 2.8$, we find from simulations^{10,12} that $\Delta \sim 16\text{K}$, which according to Ref. 27 is about three times too large for a two-component lattice to form.

A CF ground-state spin transition^{28,29} is also unlikely to explain the observed phenomena. The CF spin-Landau levels only cross above the Fermi level²⁹. Though skyrmion solid formation has been reported³⁰ from pinning modes near $\nu = 1$, at the larger ν_c^* studied here large quasihole density

would suppress skyrmion effects.

In summary, near $\nu = 1$ in WQWs, we have found a change in f_{pk} that is naturally interpreted as signature of a transition between two different solids. S2, which exists at larger $|\nu^*|$, larger n and larger w , has enhanced f_{pk} relative to the other phase. While the origin of the transition remains unclear, the possibilities, particularly of a transition in CFWS vortex number, are of fundamental importance.

Acknowledgements

We thank Jainendra Jain for illuminating discussions. The microwave spectroscopy work at NHMFL was supported through DOE grant DE-FG02-05-ER46212 at NHMFL/FSU. The National High Magnetic Field Laboratory (NHMFL), is supported by NSF Cooperative Agreement No. DMR-0654118, by the State of Florida, and by the DOE. The work at Princeton was funded through the NSF (grants DMR-1305691 and MRSEC DMR-0819860), the Keck Foundation and the Gordon and Betty Moore Foundation (grant GBMF2719).

Methods

For dc measurements the symmetry of the charge distribution about the well center was maintained using the Fourier transform of R_{xx} vs B in the Shubnikov-de Haas regime to minimize the gap, Δ , between the lowest and first excited subbands^{10,14}. For the microwave measurements, balance of the change between front and back halves of the well was maintained by biasing front and back gates such that individually each would change the carrier density by equal amounts.

Our microwave spectroscopy² technique^{9,15,30} uses a coplanar waveguide

(CPW) on the surface of a sample. A NiCr front gate was deposited on glass that was etched to space it from the CPW by $\sim 10 \mu\text{m}$. A schematic diagram of the microwave measurement technique is shown in the left panel of Fig. 1(b) and side view of the sample is shown in Fig. 1(c). From the power P transmitted through the line, we calculate the diagonal conductivity as $\sigma_{xx}(f) = (s/lZ_0) \ln(t/t_0)$, where $s = 30 \mu\text{m}$ is the distance between the center conductor and ground plane, $l = 28 \text{ mm}$ is the length of the CPW, and $Z_0 = 50 \Omega$ is the characteristic impedance without the 2DES. t_0 is the transmitted amplitude at $\nu = 1$. $\sigma_{xx}(f)$ is the difference between the conductivity and that for $\nu = 1$; just at $\nu = 1$ the conductivity is vanishing at low temperature. The microwave measurements were carried out in the low-power limit, where the measurement is not sensitive to the excitation power, and at a temperature of 60 mK. For dc transport measurements no transmission line was used; measurements were performed in a van der Pauw geometry using standard ($\simeq 30 \text{ Hz}$) lock-in technique at a temperature of about 30 mK, with front and back gates both deposited directly on the sample surfaces.

Author Contributions

A.T.H. performed the microwave measurements, analyzed the data and co-wrote the manuscript. Y.L. designed, performed and analyzed the dc experiments and did numerical simulations. B.A.M. and B.H.M. performed initial microwave measurements. L.W.E. and M.S. conceived and designed the experiment, discussed data analysis, and co-wrote the manuscript. L.N.P., K.W.W. and K.W.B. were responsible for the growth of the samples.

- [1] Lozovik, Y. E. & Yudson, V. Crystallisation of a two dimensional electron gas in magnetic field. *JETP Letters* **22**, 11 (1975).
- [2] Andrei, E. Y. *et al.* Observation of a magnetically induced Wigner solid. *Phys. Rev. Lett.* **60**, 2765-2768 (1988).
- [3] Goldman, V. J., Santos, M., Shayegan, M. & Cunningham, J. E. Evidence for two-dimensional quantum Wigner crystal. *Phys. Rev. Lett.* **65**, 2189–2192 (1990).
- [4] H.-W. Jiang *et al.* Quantum liquid versus electron solid around $\nu = 1/5$ Landau-level filling. *Phys. Rev. Lett.* **65**, 633 (1990).
- [5] Williams, F.I. B. *et al.* Conduction threshold and pinning frequency of magnetically induced Wigner solid. *Phys. Rev. Lett.* **66**, 3285-3288 (1991).
- [6] Yang, K., Haldane, F. D. M. & Rezayi, E. H. Wigner crystals in the lowest Landau level at low-filling factors. *Phys. Rev. B* **64**, 081301 (2001).
- [7] Archer, A. C., Park, K. & Jain, J. K. Nature of the crystal phase between $1/5$ and $2/9$ fractional Hall liquids. *Phys. Rev. Lett.* **111**, 146804 (2013).
- [8] Shayegan, M. in *Perspectives in quantum Hall effects*, edited by S. Das Sarma and A. Pinczuk, 343 (Wiley-Interscience, New York, 1997).
- [9] Chen, Y. *et al.* Microwave resonance of the 2D Wigner crystal around integer Landau fillings. *Phys. Rev. Lett.* **91**, 016801 (2003).
- [10] Liu, Y., Shabani, J. & Shayegan, M. Stability of the $q/3$ fractional quantum Hall states. *Phys. Rev. B* **84**, 195303 (2011).
- [11] Liu, Y. *et al.* Observation of reentrant integer quantum Hall states in the lowest Landau level. *Phys. Rev. Lett.* **109**, 036801 (2012).
- [12] Shayegan, M., Manoharan, H. C., Suen, Y. W., Lay, T. S. & Santos, M. B. Correlated bilayer electron states. *Semiconductor Science and Technology* **11**, 1539 (1996).

- [13] Manoharan, H. C., Suen, Y. W., Santos, M. B. & Shayegan, M. Evidence for a bilayer quantum Wigner solid. *Phys. Rev. Lett.* **77**, 1813–1816 (1996).
- [14] Suen, Y. W., Manoharan, H. C., Ying, X., Santos, M. B. & Shayegan, M. Origin of the $\nu = 1/2$ fractional quantum Hall state in wide single quantum wells. *Phys. Rev. Lett.* **72**, 3405 (1994).
- [15] Chen, Y. P. *et al.* Evidence for two different solid phases of two-dimensional electrons in high magnetic fields. *Phys. Rev. Lett.* **93**, 206805 (2004).
- [16] Fukuyama, H. & Lee, P. A. Pinning and conductivity of two-dimensional charge-density waves in magnetic fields. *Phys. Rev. B* **18**, 6245-6252 (1978).
- [17] Fertig, H. A. Electromagnetic response of a pinned Wigner crystal. *Phys. Rev. B* **59**, 2120–2141 (1999).
- [18] Chitra, R., Giamarchi, T. & Le Doussal, P. Pinned Wigner crystals. *Phys. Rev. B* **65**, 035312 (2001).
- [19] Fogler, M. M. & Huse, D. A. Dynamical response of a pinned two-dimensional Wigner crystal. *Phys. Rev. B* **62**, 7553–7570 (2000).
- [20] Li, C.-C. *et al.* Microwave resonance and weak pinning in two-dimensional hole systems at high magnetic fields. *Phys. Rev. B* **61**, 10905–10909 (2000).
- [21] Price, R., Zhu, X., Das Sarma, S. & Platzman, P. M. Laughlin-liquid~Wigner-solid transition at high density in wide quantum wells. *Phys. Rev. B* **51**, 2017–2020 (1995).
- [22] Gervais, G. *et al.* Competition between a fractional quantum Hall liquid and bubble and Wigner crystal phases in the third Landau level. *Phys. Rev. Lett.* **93**, 266804 (2004).
- [23] Lilly, M. P. *et al.* Evidence for an anisotropic state of two-dimensional electrons in high Landau levels. *Phys. Rev. Lett.* **82**, 394 (1999). The RIQHE was first seen in higher Landau levels, and is understood as a signature of bubble phases. Such phases are not predicted for the lowest Landau level, as discussed in Ref. 11.

- [24] Chang, C.-C., Jeon, G. S. & Jain, J. K. Microscopic verification of topological electron-vortex binding in the lowest Landau-level crystal state. *Phys. Rev. Lett.* **94**, 016809 (2005).
- [25] Narevich, F., Murthy, G. & Fertig, H. A. Hamiltonian theory of the composite-fermion Wigner crystal. *Phys. Rev. B* **64**, 245326 (2001).
- [26] Yi, H. & Fertig, H. A. Laughlin-Jastrow-correlated Wigner crystal in a strong magnetic field. *Phys. Rev. B* **58**, 4019 (1998).
- [27] Narasimhan, S. & Ho, T.-L. Wigner-crystal phases in bilayer quantum Hall systems. *Phys. Rev. B* **52**, 12291 (1995).
- [28] Du, R. R. *et al.* Fractional quantum Hall effect around $\nu = 3/2$: Composite fermions with a spin. *Phys. Rev. Lett.* **75**, 3926 (1995).
- [29] Yeh, A. S. *et al.* Effective mass and g factor of four-flux-quanta composite fermions. *Phys. Rev. Lett.* **82**, 592 (1999).
- [30] Zhu, H. *et al.* Pinning-mode resonance of a skyrme crystal near Landau-Level filling Factor $\nu = 1$. *Phys. Rev. Lett.* **104**, 226801 (2010).